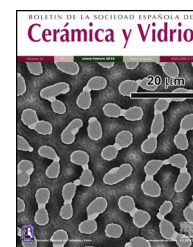




BOLETIN DE LA SOCIEDAD ESPAÑOLA DE  
**Cerámica y Vidrio**

[www.elsevier.es/bsecv](http://www.elsevier.es/bsecv)



## Original

# Synthesis and study of europium doped BaI<sub>2</sub> in glass ceramic form

Tatsiana Salamakha<sup>a,\*</sup>, Maksym Buryi<sup>b</sup>, Ekaterina Trusova<sup>c</sup>, Yauhen Tratsiak<sup>a</sup>

<sup>a</sup> Research Institute for Physical Chemical Problems, Belarusian State University, Minsk, Belarus

<sup>b</sup> Institute of Physics of the Czech Academy of Science, Prague, Czech Republic

<sup>c</sup> Belarusian State Technological University, Minsk, Belarus

### ARTICLE INFO

#### Article history:

Received 14 January 2020

Accepted 25 April 2020

Available online xxx

#### Keywords:

Luminescence

Eu<sup>2+</sup>

Glass ceramics

EPR

Barium iodide

#### Palabras clave:

Luminiscencia

Eu<sup>2+</sup>

Vitrocéramica

RPE

Yoduro de bario

### ABSTRACT

Present paper reports an approach to BaI<sub>2</sub>:Eu<sup>2+</sup> glass ceramics fabrication from a powder route. The structural, morphological, luminescent and paramagnetic properties of the materials synthesized this way have been investigated. X-ray diffraction analysis made evidence for the glass ceramics containing BaI<sub>2</sub>·2H<sub>2</sub>O and BaI<sub>2</sub> inclusions when 50 wt.% of the starting iodide powder had been used in the synthesis process. According to scanning electron microscopy, only two samples demonstrated presence of ceramics particles inside: those with initial mix of 25 and 50 wt.% of the BaI<sub>2</sub>:Eu<sup>2+</sup>. Photoluminescence spectra could be measured only in these samples. They were multicomponent as compared to the single band spectrum observed in the BaI<sub>2</sub>:Eu<sup>2+</sup> powder. Altogether this indicates europium distribution over several places with different environments in the materials. BaI<sub>2</sub> dissolution in the glass matrix is confirmed further by electron paramagnetic resonance measurements. They have shown that the Eu<sup>2+</sup> ions predominantly stay in the glass avoiding ceramic grains. Only negligibly small amount presumably occupies the ceramic part in the sample with the initial 50 wt.% part of the BaI<sub>2</sub> powder. The Eu<sup>2+</sup> → Eu<sup>3+</sup> charge transformation under 442 nm laser light irradiation has been observed in the glass ceramics as well.

© 2020 SECV. Published by Elsevier España, S.L.U. This is an open access article under the CC BY-NC-ND license (<http://creativecommons.org/licenses/by-nc-nd/4.0/>).

### Síntesis y estudio de BaI<sub>2</sub> dopado con europio en forma de vitrocerámica

#### RESUMEN

Este artículo informa sobre el enfoque de síntesis de BaI<sub>2</sub>:Eu<sup>2+</sup> vitrocerámica a partir de una ruta de polvo. Se han investigado las propiedades estructurales, morfológicas, luminiscentes y paramagnéticas de los materiales sintetizados de esta manera. El análisis de la difracción de rayos X había demostrado las vitrocerámicas que contienen inclusiones de BaI<sub>2</sub>·2H<sub>2</sub>O y BaI<sub>2</sub> cuando el 50% en peso del polvo de yoduro se había utilizado en el proceso de síntesis. Según la microscopía electrónica de barrido, solo dos muestras demostraron la presencia

\* Corresponding author.

E-mail address: [solomakha.tanja@gmail.com](mailto:solomakha.tanja@gmail.com) (T. Salamakha).

<https://doi.org/10.1016/j.bsecv.2020.04.002>

0366-3175/© 2020 SECV. Published by Elsevier España, S.L.U. This is an open access article under the CC BY-NC-ND license (<http://creativecommons.org/licenses/by-nc-nd/4.0/>).

de partículas de cerámica adentro: aquellas con una cantidad inicial del 25 y 50% en peso del  $\text{BaI}_2:\text{Eu}^{2+}$ . Los espectros de fotoluminiscencia solo se pudieron medir en estas muestras. Eran multicomponentes en comparación con el espectro de banda única observado en el polvo  $\text{BaI}_2:\text{Eu}^{2+}$ . En conjunto, esto indica la distribución de europio en varios lugares con diferentes ambientes en los materiales. La disolución de  $\text{BaI}_2$  en la matriz de vidrio se confirma, además, por mediciones de resonancia paramagnética electrónica. Han demostrado que los iones de  $\text{Eu}^{2+}$  permanecen predominantemente en el vidrio, evitando los gránulos de cerámica. Solo una cantidad insignificamente pequeña ocupa presumiblemente la parte cerámica en la muestra con el 50% en peso del polvo inicial de  $\text{BaI}_2$ . La transformación de carga de  $\text{Eu}^{2+} \rightarrow \text{Eu}^{3+}$  bajo irradiación de luz láser de 442 nm también se ha observado en la vitrocerámica.

© 2020 SECV. Publicado por Elsevier España, S.L.U. Este es un artículo Open Access bajo la licencia CC BY-NC-ND (<http://creativecommons.org/licenses/by-nc-nd/4.0/>).

## Introduction

Development of new cheap and effective luminescent materials is one of the demanding tasks in materials science. It is inspired by everlasting search for improvement in the numerous fields of human's activity and life where such materials find applications as detectors transforming incident high energy radiation into light of the required spectral range. These fields are: high energy physics, photonics, medicine, lighting, security, agriculture and others [1–3]. The most prominent and effective representatives of the promising phosphors are halide based compounds doped with rare earths,  $\text{Eu}^{2+}$ ,  $\text{Eu}^{3+}$ ,  $\text{Dy}^{3+}$ ,  $\text{Tb}^{3+}$ ,  $\text{Ce}^{3+}$ , etc. depending on the required emission wavelength [4–6]. Glasses, ceramics and glass ceramics are perspective as luminescent materials due to thermal and radiation stability, variable optical properties and sufficient optical tunability [7–10]. Furthermore, it is much easier to obtain materials in a glass ceramic form in comparison with single crystals since they require lower fabrication costs [1] and allow to combine glass and crystalline properties [2].

In general, glass ceramics synthesis can be accomplished in two ways: (i) direct growth of crystalline phase in glass matrix during its crystallization, including sol-gel process in the primary stage [4,11–13]; (ii) mixing of glass and phosphor powders with subsequent thermal treatment (PiG) [14] (additional information about powder route can also be found in [15]). Both technologies have certain peculiarities related to the resulting phosphor composition. The former suffers from the formation of competitive additional phases during crystallization. To avoid them, thorough control of initial glass compositions or crystallization conditions allowing to receive only one crystalline phase is needed. This, however, may be a difficult task. In the second technology the possibility of new compounds formation due to the chemical reaction between glass and crystalline materials must be taken into account. The shape and wettability of the crystalline particles surface in the glass medium are also important, because this can be the source of strong nonuniformity of the crystalline particles distribution in a glass matrix. The decrease of transparency or coloration of the glass ceramics can be expected in this case. Despite this, the glass ceramics with crystallites homogeneously spread over the glass matrix may be obtained [16]. Among the other

good qualities, the glass matrix has a moisture protecting function, exceedingly useful when the ceramic particles are hygroscopic. Moreover, implementation of the glass ceramics diminishes the problem of structural anisotropy [1,7].

Among all the iodides of alkaline-earth elements,  $\text{BaI}_2$  has the highest  $Z_{\text{eff}}$  and broad bandgap of about 5 eV, comparable to that of  $\text{SrI}_2$ . Oppositely to the  $\text{SrI}_2$  it is much less hygroscopic. This allows its easier production especially in the glass ceramics form. Along with the absence of radioactive isotopes affecting the background all this makes it prospective not only as phosphor [17,18] but also as scintillation material for various applications (homeland security, nuclear control, high-energy physics, etc.) [2,19,20].

Unfortunately, structural anisotropy is serious barrier in  $\text{BaI}_2$  production. The single crystal growth of  $\text{BaI}_2:\text{Eu}$  is expensive and long lasting process. Moreover, currently it is not possible to obtain transparent samples of large volume due to anisotropy, which leads to certain difficulties for their practical implementation. It should also be noted that optical transparency for such materials is critical, since it is important to collect the signal from the entire volume and not only from the surface.

Normally, barium iodide melts with decomposition at 711 °C. Some studies, however, have shown the possibility of the barium iodide-based glass ceramic materials production at higher melting temperatures [21]. Therefore, understanding the processes occurring during this glass ceramics synthesis is important and interesting.

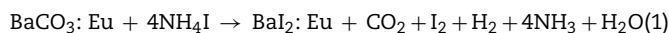
The present work is thus aiming at the development and testing of the reliable and cheap technique for the europium doped barium iodide glass ceramics fabrication. This includes detailed investigation of the glass ceramics synthesis on the basis of the barium iodide powder to glass host ratio. Europium doped barium iodide glass ceramics structural, morphological, luminescent and paramagnetic properties will appear in the crosshair of rigorous investigation by X-rays, optical and electron paramagnetic resonance (EPR) methods. In particular, EPR will check the  $\text{Eu}^{2+}$  distribution and incorporation in the crystalline lattice and glass host. With this purpose the samples were prepared employing the two-step approach: primarily synthesized barium iodide particles activated with  $\text{Eu}^{2+}$  were immersed into the glass matrix. The proposed technology can also be applied to other alkali-earth halides glass ceramics manufacturing, in perspective.

## Experimental procedure

$\text{Ba}(\text{NO}_3)_2$ ,  $\text{Eu}(\text{NO}_3)_3 \cdot 6\text{H}_2\text{O}$ ,  $\text{NH}_4\text{HCO}_3$ ,  $\text{NH}_4\text{I}$ ,  $\text{BaCO}_3$  and  $\text{H}_3\text{BO}_3$  were used as starting materials. All reagents were of analytical grade.  $\text{BaI}_2$  was prepared by using 2 stages method described earlier [18]: the first involved the synthesis of the  $\text{BaCO}_3\text{:Eu}$  (precursor) converted into the  $\text{BaI}_2\text{:Eu}$  in the second stage.

$\text{BaCO}_3\text{:Eu}$  powder was obtained by reverse precipitation. At first the required quantity of 0.1 M  $\text{Eu}(\text{NO}_3)_3$  solution was added into the 0.2 M  $\text{Ba}(\text{NO}_3)_2$ . It was enough to ensure 2 at.% of  $\text{Ba}^{2+}$  ions to be replaced by  $\text{Eu}^{2+}$ . The mixture of nitrates was then added dropwise into 1.2 M solution of  $\text{NH}_4\text{HCO}_3$  under constant stirring at room temperature. The resulting  $\text{BaCO}_3\text{:Eu}$  precipitate was isolated by centrifugation, washed 2 times with distilled water and dried in air at 80 °C for 12 h.  $\text{BaCO}_3\text{:Eu}$  and  $\text{NH}_4\text{I}$  powders had been mixed in the agate mortar and then transferred into a quartz boat which was placed into a quartz tube with subsequent argon (Ar) flux for 10 min. The tube was then moved into the furnace preheated up to 400 °C and annealed at this temperature for 30 min under constant Ar flow. After that the sample was spontaneously cooled down to the room temperature (~50 °C/min) in a quartz tube under the Ar flow. The obtained light-gray powder was introduced into a container and sealed tightly. The sample was designated as the "Sample 0".

The whole process can be described by the following equation:



It should be mentioned that influence of the precursor morphology and Eu-ions concentration on the structural and luminescent properties of the  $\text{BaI}_2\text{:Eu}$  powders have been investigated previously [18,22].

To obtain the glass with the composition of 60 wt.% BaO and 40 wt.%  $\text{B}_2\text{O}_3$  the melt-quenching technique was used.  $\text{H}_3\text{BO}_3$  was taken with 15% excess. The glass synthesis was carried out in porcelain crucibles within an electric furnace at 1000 °C during 1 h. The glass melt was cast onto a metal plate. The resulting glass was transparent and colorless.

The mixture of  $\text{BaI}_2$  and  $\text{BaO-B}_2\text{O}_3$  glass grinded to the fine powder containing 0, 5, 10, 25, 50 wt.% of  $\text{BaI}_2$  was introduced into a quartz tube ventilated with Ar flux for 10 min in the process of the glass ceramics synthesis. The tube was then placed into a furnace preheated to 200 °C and held there for 15 min to release the crystallization water. Then the 900 °C temperature was set for another 15 min with the ~50 °C/min heating rate. After the synthesis, the glass ceramics samples were removed from the furnace and cooled down. All stages of the glass ceramic synthesis were carried out in Ar atmosphere. The heating rate was high enough to prevent losses of the barium iodide due to its decomposition. Designations of the samples with different content of the  $\text{BaI}_2$  powder are listed in Table 1.

## Characterization techniques

X-ray diffraction patterns of the synthesized samples were collected by PANalytical Empyrean X-ray diffractometer with

**Table 1 – Designations of the obtained glass ceramics samples with the given amount of the  $\text{BaI}_2$  powder used in the synthesis.**

Sample	0	1	2	3	4	5
$\text{BaI}_2$ , wt.%	100	0	5	10	25	50

Cu-K( $\alpha$ ) radiation source ( $\lambda = 1.5406 \text{ \AA}$ ) in the  $2\theta$  range of 10–70°. To prevent the contact of a  $\text{BaI}_2$  sample with water from atmosphere it was placed in a holder between two polyethylene films (on the X-ray diffraction pattern they show reflections with maxima at 21.6° and 23.8°  $2\theta$ ). The size of the coherent scattering region (CSR) and microstress values were determined from full width at half maxima (FWHM) of the X-ray diffraction (XRD) lines approximated by the Voigt functions using Williamson–Hall method [23]. Usual corrections for the Cu-K( $\alpha$ ) radiation were taken into account. The processing of data was made in Fityk, WinPLOTR-2006 and DICVOL06 programs of FullPROF.

Fourier-transform infrared spectroscopy (FTIR) was carried out using Perkin Elmer spectrometer Spectrum Two with a UATR TWO unit (Diamond), 64 scans, 4  $\text{cm}^{-1}$  resolution, between 400 and 4000  $\text{cm}^{-1}$ .

Morphology of the glass ceramics was studied by scanning electron microscope (SEM) Hitachi SU-70 with the 1000 and 10,000 magnification. To study the  $\text{BaI}_2$  powder morphology the SEM on a LEO-1420 was used.

Room temperature photoluminescence (PL) measurements were provided by Jobin Yvon Fluoromax 2 spectrofluorimeter. In the case of powder, the PL and photoluminescence excitation (PLE) spectra were collected from ~1 mm-thick layers of powder placed onto a quartz plate.

EPR measurements were carried out in the X-band (~9.4 GHz) with a commercial Bruker X/Q-band E580 FT/CW ELEXSYS spectrometer within the 3.6–296 K temperature range using an Oxford Instruments ESR900 continuous flow cryostat. UV irradiation (330 nm) was delivered using a mercury high-pressure arc lamp.

## Results and discussion

The XRD pattern of the sample 0 is shown in Fig. 1. It exhibits strong reflections characteristic for the  $\text{BaI}_2$  (Powder Diffraction File (PDF) № 73-1849). The much weaker and broader ones, marked with asterisks, were referred to the  $\text{BaI}_2 \cdot \text{H}_2\text{O}$  (PDF № 39-1300). The content of the  $\text{BaI}_2 \cdot \text{H}_2\text{O}$  is thus much smaller as compared to the pure  $\text{BaI}_2$ . Obviously, the hydrated iodide is the result of the sample interaction with water vapor.

The XRD patterns of the glass ceramic samples with different content of  $\text{BaI}_2$  powder are shown in Fig. 1. The samples 1–4 are amorphous and do not show any reflections. This is, most probably, because of thermal decomposition of the  $\text{BaI}_2$  or dissolution by glass matrix during the synthesis process. At any rate the quantity and size of the ceramics particles were below the XRD detection abilities. Oppositely, the reflections originating from pure  $\text{BaI}_2$  (PDF № 73-1849) were detected in the sample 5. This makes clear evidence for the shielding effect of the glass matrix preventing the  $\text{BaI}_2$  ceramics from contact with water vapor. However, the presence and domination of  $\text{BaI}_2 \cdot 2\text{H}_2\text{O}$  (PDF № 31-0145) reflections in the sample

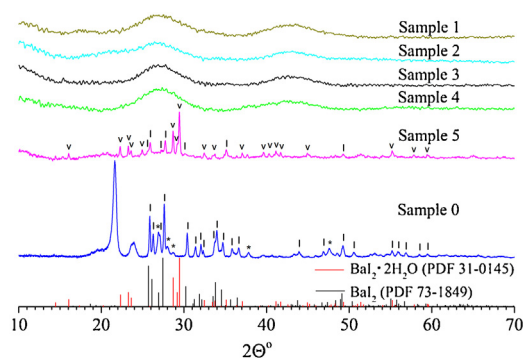


**Fig. 1** – XRD patterns of the sample 0 and glass ceramic samples 1–5 with different content of BaI<sub>2</sub> powder. The BaI<sub>2</sub>·H<sub>2</sub>O reflections (PDF № 39–1300) are marked with asterisks (\*), BaI<sub>2</sub>·2H<sub>2</sub>O (PDF № 31–0145) – with (v), BaI<sub>2</sub> (PDF № 73–1849) – with (l), respectively. Broaden reflections with the maxima at 21.6° and 23.8° originate from a polyethylene film. The sample numbers correspond to Table 1.

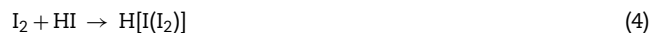
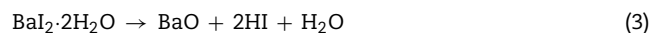
5 were observed (see Fig. 1). The prevalence of BaI<sub>2</sub>·2H<sub>2</sub>O phase is, most probably, the result of sample grinding for XRD analysis. The process partly breaks the glass matrix protection (microcracks occur) exposing the ceramic particles (highly hygroscopic [24]) to the surrounding atmosphere. On the other hand, the simultaneous presence of BaI<sub>2</sub> and BaI<sub>2</sub>·2H<sub>2</sub>O phases in the sample 5 in contrast to the samples 1–4 can be explained by larger amount of BaI<sub>2</sub> powder used in the synthesis process. This could lead to the not fully completed decomposition.

Calculated values of the unit cell parameters, CSR size and microstress ( $\epsilon$ ) are listed in Table 2 for the sample 0 and sample 5. Cell parameters are in a good agreement with the tabulated data (PDF № 73–1849) for the BaI<sub>2</sub>. Due to the very small content of the BaI<sub>2</sub>·H<sub>2</sub>O phase in the sample 0 (see Fig. 1) and its low crystallinity it was unable to perform the calculation of its cell parameters.

The obtained values of the unit cell parameters are in agreement with the tabulated data for the BaI<sub>2</sub> (PDF № 73–1849) and BaI<sub>2</sub>·2H<sub>2</sub>O (PDF № 31–0145) in the sample 5. It can be seen in Table 2, that the values of the glass ceramic BaI<sub>2</sub> cell parameters differ from the pure powder, most likely, due to the dissolution in the glass matrix. Estimated CSR and microstress values for the BaI<sub>2</sub> phase in the sample 5 are lower by the factors of 1.7 and 2.9, respectively, as compared to the sample 0. This may be in connection with the decreased iodide particles size due to their decomposition or dissolving and rearrang-

ing of defects at the stage of glass ceramic synthesis at high temperature.

The whole decomposition process may be described by the following equations:



The presence of O<sub>2</sub> in the samples is, most probably, related to the surface absorption from air during the procedure of the glasses grinding.

On the other hand, the microstress value of the BaI<sub>2</sub> phase is lower approximately 3 times in the sample 5 as compared to the sample 0. It cannot be explained solely by the BaI<sub>2</sub> decomposition since the glass ceramics synthesis is carried out at higher temperatures. Therefore, one could assume the BaI<sub>2</sub> particles formation from BaO and H[I(I<sub>2</sub>)] or HI presented in the glass ceramics and as a result having more rigid packing than the sample 0. This assumption may be partially confirmed also by the same XRD patterns of the sample 5 and sample 0 (see Fig. 1). It is partially confirmed also by the changed BaI<sub>2</sub> particles morphology (discussed further in text).

The FTIR spectra measured in the samples 0–5 as well as in BaCO<sub>3</sub>:Eu are shown in Fig. 2(a). The BaCO<sub>3</sub> sample exhibits absorption bands at 853 and 1426 cm<sup>-1</sup> related to the –CO<sub>3</sub><sup>2-</sup> groups. The FTIR spectrum of the sample 0 [see Fig. 2(b)] demonstrates strong absorption peaks with the maxima at around 1605 cm<sup>-1</sup> and in the 3000–3700 cm<sup>-1</sup> range, due to stretching and bending vibrations of water molecules, respectively. This makes evidence for the BaI<sub>2</sub>·H<sub>2</sub>O hydrated phase existence. Weak absorption band with the maximum at ~1400 cm<sup>-1</sup>, most probably, belongs to the –CO<sub>3</sub><sup>2-</sup> group presented in the form of BaCO<sub>3</sub> (see Fig. 2). This is an evidence for the incomplete process described by Eq. (1).

Peaks characteristic for water molecules, and others, of lower intensity, were detected within the 700–1400 cm<sup>-1</sup> range in the sample 5. They were associated with the oscillations of bonds in the CO<sub>2</sub>, NH<sub>3</sub>, –CO<sub>3</sub><sup>2-</sup>, –IO<sub>3</sub><sup>-</sup> and BaO [25] being residuals of the starting materials and/or by-products of the BaI<sub>2</sub> and glass ceramics synthesis. The CO<sub>2</sub> and NH<sub>3</sub> were released during the BaI<sub>2</sub>:Eu synthesis according to Eq. (1); the –CO<sub>3</sub><sup>2-</sup> groups are the part of the BaCO<sub>3</sub>, one of chemicals used for the glass production; the BaO is a glass network component and the –IO<sub>3</sub><sup>-</sup> groups were created as the product of the iodide oxidation [26]. The BaI<sub>2</sub> bonds vibrations in the samples 0–5 are situated in the unreachable range of FTIR (<200 cm<sup>-1</sup>).

**Table 2** – Unit cell parameters, CSR sizes and microstress values for the synthesized sample 0, glass ceramic sample 5 and BaI<sub>2</sub> (from database).

Sample	Compound	Space group	a, Å	b, Å	c, Å	$\alpha$ , °	$\beta$ , °	$\gamma$ , °	CSR, nm	$\epsilon$ , 10 <sup>-5</sup>
5	BaI <sub>2</sub> ·2H <sub>2</sub> O	P2/m	11.1296(176)	7.6151(4)	8.6434(4)	90.000	112.4120(97)	90.000	45.7	4.87
	BaI <sub>2</sub>	Pmmm	10.7110(5)	8.9066(6)	5.3030(3)	90.000	90.0000	90.000	31.1	3.09
0	BaI <sub>2</sub>	Pmmm	10.6851(3)	8.9128(2)	5.3007(2)	90.000	90.0000	90.000	54.0	8.86
	BaI <sub>2</sub>	Pbnm	10.6800	8.9040	5.2980	90.000	90.0000	90.000	–	–



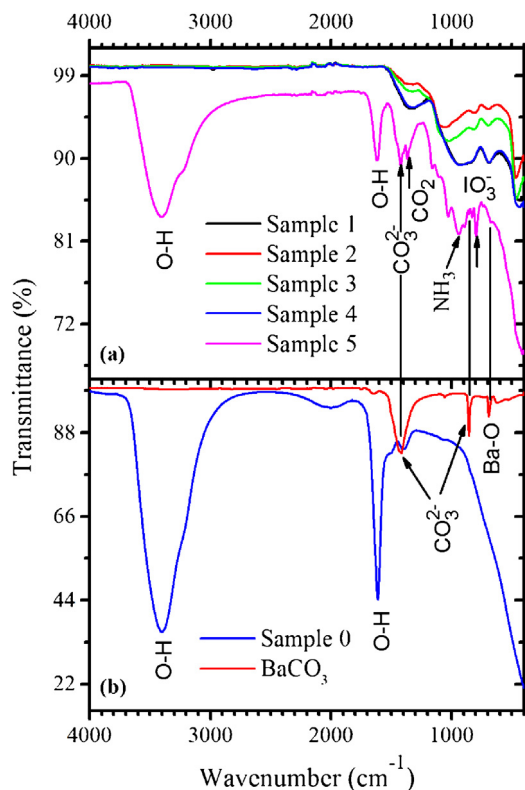


**Fig. 2 – (a) FTIR spectra of the samples 1–5; (b) FTIR spectra of the sample 0 and BaCO<sub>3</sub>.**

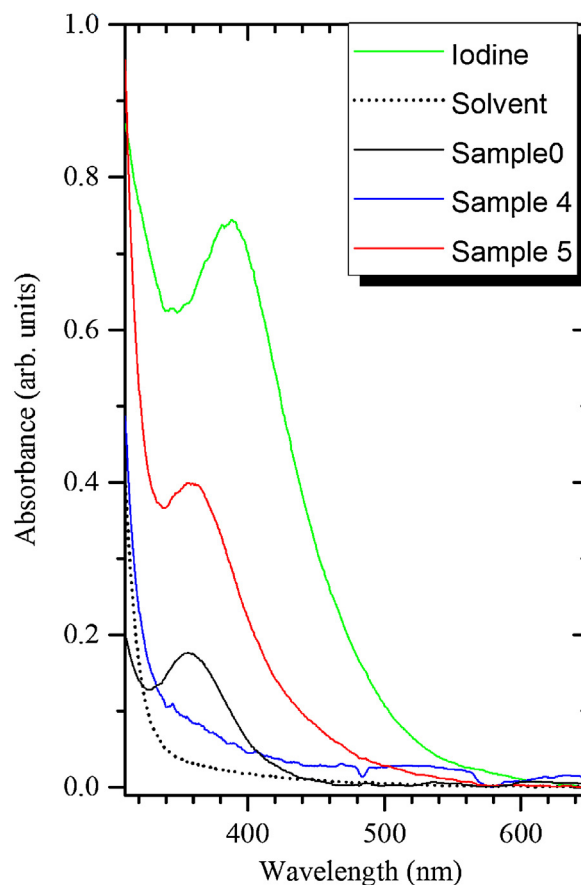


**Fig. 3 – Absorption spectra of the samples 0, 4, 5, solvent (immersion oil) and 4% iodine solution in the solvent.**

Absorption spectra of the samples 0, 4 and 5 are demonstrated in Fig. 3. The band peaking at 360 nm can be attributed to the  $I_3^-$  ions as described in previous work [18]. It is stronger in the sample 5 as compared to the sample 4 because the former contains much larger amount of the BaI<sub>2</sub> phase. The more  $I_2$  is thus expected to release during the decomposition of the BaI<sub>2</sub> in the synthesis process or during the glass ceramics storing. The  $I_3^-$  accumulation in the glass ceramics may also occur in the process described in Eqs. (2)–(4).

SEM images of the samples 0, 4 and 5 are shown in Fig. 4. It can be seen that the sample 0 consists of the 1–2  $\mu\text{m}$  large aggregates densely packed [see Fig. 4(a, b)] whereas the sample 4 and sample 5 exhibit presence of distinct inclusions (marked with yellow arrows) largely spaced. They appear to be spherical in the sample 4 with the average diameter of 500 nm [see Fig. 4(c, d)]. Oppositely, the particles are smaller of rather

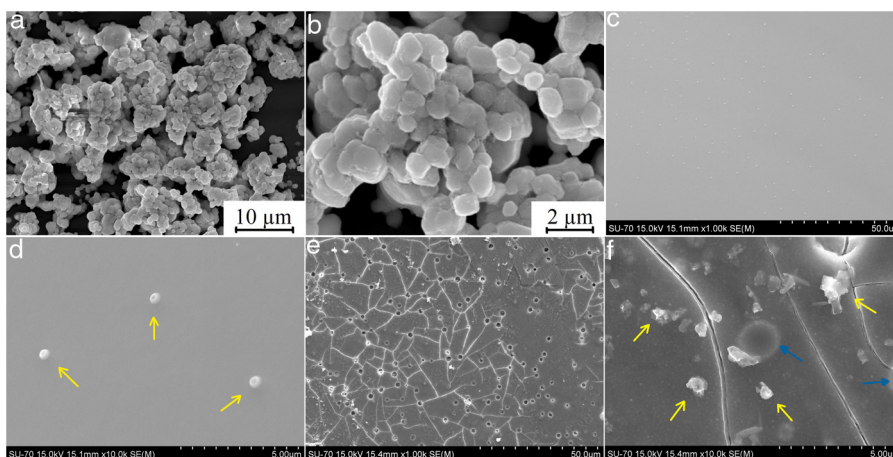


**Fig. 4 – SEM images of the samples 0 (a, b), 4 (c, d), and 5 (e, f). Yellow arrows point out ceramic particles whereas the blue ones indicate cracks and pores (bubbles).**

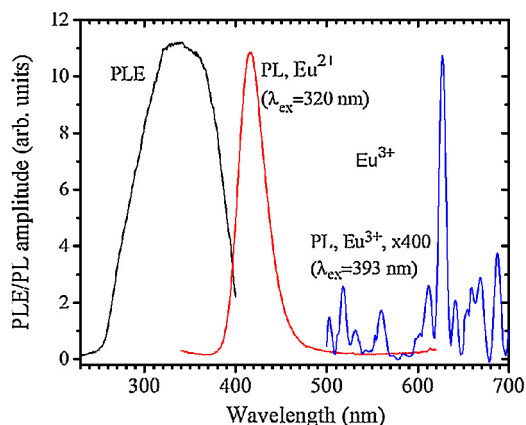


**Fig. 5** – PLE ( $\lambda_{em} = 415$  nm) and PL spectra ( $\lambda_{ex} = 320$  nm and  $\lambda_{ex} = 393$  nm) for the  $BaI_2:Eu^{2+}$  powder. The PL spectrum for the  $\lambda_{ex} = 393$  nm was 400 times magnified.

irregular shape in the sample 5 [see Fig. 4(e, f)]. Moreover, they have tendency to coalesce, creating relatively large agglomerations which size is ranging from approximately 0.5 to 2  $\mu m$ . On the basis of XRD analysis above proving the presence of the  $BaI_2$  in the samples 4 and 5, the observed particles were deduced to be the  $BaI_2$  ceramic grains. Smaller size and ragged edges of the ceramic grains in the sample 5 can be the result of the  $BaI_2$  dissolution specifics in the glass matrix as compared to the Sample 0 (see the microstress values above). Besides, cracks and round-shaped pores [or bubbles, marked with blue arrows in Fig. 4(f)] of the 2–2.5  $\mu m$  size were observed in the sample 5. They are formed due to intensive isolation of the gaseous products during the synthesis process. Note, that the samples 1–3 do not demonstrate the particles presence in the glass matrices at all. This is expected to be the result of their total decomposition or dissolution by glass matrix.

The PL and PLE spectra of the sample 0 are shown in Fig. 5. The broad PLE band within the 255–400 nm was referred to the  $Eu^{2+} 4f \rightarrow 5d$  transition according to [27].

A PL spectrum in the sample 0 ( $\lambda_{ex} = 320$  nm) is composed of a single narrow band with nearly symmetric lineshape centered at 415 nm. It has been referred to the inter-configurational  $4f^6 5d^1 \rightarrow 4f^7$  radiation transition of the  $Eu^{2+}$  in

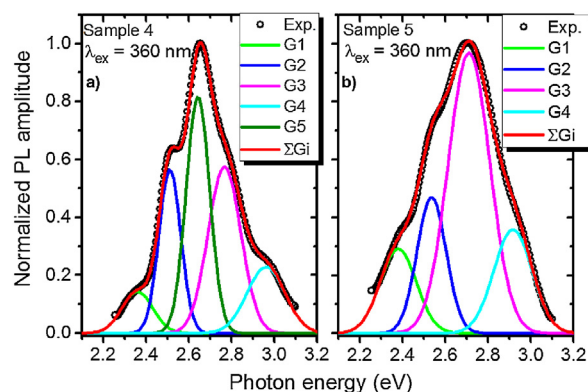


**Fig. 7** – Decomposition of the observed PL spectra in the sample 4 (a) and sample 5 (b) into components by calculated Gaussians (G1–G5) and their sums ( $\sum Gi$ ).

the  $BaI_2$  structure [18]. Very weak  $Eu^{3+}$  spectrum ( $\lambda_{ex} = 393$  nm), its intensity is 400 times lower than that of the  $Eu^{2+}$ , was resolved due to specific and commonly known transitions (see Fig. 5). This indicates insignificant amount of the  $Eu^{3+}$  present in the barium iodide sample [22,28]. PLE and PL spectra measured in the samples 4 and 5 are shown in Fig. 6(a) and (b) normalized to the maximum signal intensity in the sample 5 (naturally stronger because of 2 times increased  $BaI_2$  content as compared to the sample 4). Normalized to the maximum amplitude they are shown in Fig. 6(c). The spectra are obviously complex. For example, in the sample 4 PL spectrum at least five strongly overlapped bands can be distinguished whereas in the sample 5 only four compared to the sample 0 (see Fig. 5). To resolve the single components, the experimental spectra have been fitted with the sum of standard Gaussian peaks according to the expression:  $Gi = A_i / FWHM_i \sqrt{\pi/4 \ln 2} \exp(-4 \ln 2 ((E - E_i)^2 / FWHM_i^2))$ , where  $A_i$ ,  $E_i$  and  $FWHM_i$  are the area under the single curve, maximum energy, and full width at half maximum, respectively. It is shown in Fig. 7. The parameters of fit are listed in Table 3. It seems that the spectra have G1–G4, four components in common, whereas the fifth one, G5, is specifically present only in the sample 4. The bands are narrower in the sample 4 except for the G4 one, which is more or less the same in both

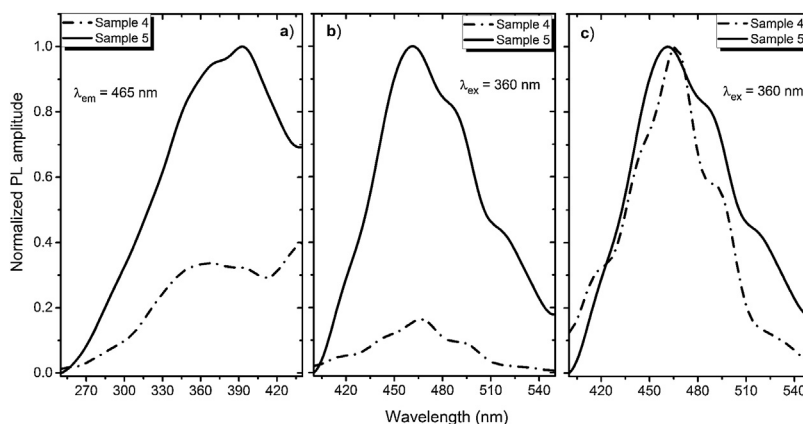


**Fig. 6** – (a) PLE ( $\lambda_{em} = 465$  nm) and (b) PL spectra ( $\lambda_{ex} = 360$  nm) of the samples 4 and 5 normalized to the amplitude in the sample 5. (c) PL spectrum in the samples 4 and 5 normalized to the maximum amplitude each.

cases. Since the correlation between these PL peaks (except for the G5) intensity and the  $BaI_2$  content was observed [see Fig. 6(a,b)], all the G1–G4 peaks were attributed to the  $Eu^{2+}$  in different local environments. It is known that the spectral position of the  $Eu^{2+}$  luminescence, in general, depends on its local ligand surrounding [29,30]. The rest of samples exhibited no PL signals.

The 422 nm peak which remains the same as to the FWHM in both samples (G4, Table 3) can be attributed to the  $Eu^{2+}$  emission from the  $BaI_2$  and/or  $BaI_2 \cdot nH_2O$  structures ( $n=1,2$ ) in the glass ceramics [31]. Its 7 nm shift with respect to the sample 0 (maximum at 415 nm) is almost within the 5 nm instrumental error of the spectrometer. However, the structural modification of the  $BaI_2$ -based particles in the glass matrix obviously affecting cell parameters values (Table 2) can also be the factor affecting  $Eu^{2+}$  emission spectral position. The shift of the excitation wavelength from 320 nm (for sample 0) to 360 nm (for samples 4 and 5) has been observed. The 453 nm band (G3, Table 3) has been referred to the  $Eu^{2+}$  in  $EuI_2$  phase [32,33] the expected byproduct of the glass ceramics synthesis according to Eq. (1) [32]. It is red shifted by approximately  $13 \pm 5$  nm off the regular  $Eu^{2+}$  emission observed in the  $EuI_2$  at 440 nm [33]. In general, its position is sensitive to external pressure [32]. Therefore, the offset can be expected to be due to the structural modification mentioned above. Lack of the characteristic  $EuI_2$  reflections in XRD patterns (see Fig. 1) could be explained by the low phase content in the sample, below the sensitivity level. The 523 nm peak (G1, Table 3) may originate from the  $Eu^{2+}$  ions perturbed by, for instance,  $Eu^{3+}$  in some structure, maybe some kind of the  $Ba_xEu_{1-x}I_2$  solid solution. The 515 nm peak has been reported previously in the  $EuI_2$  as the regular  $Eu^{2+}$ , probably disturbed by the  $Eu^{3+}$  [33].

The 492 nm band (G2, Table 3) was expected to originate from the glass or the ceramics-glass boundary because of the barium iodide dissolution. Particles dissolving strongly affect the glass medium composition initially close to a single particle, modifying it. This process is caused by the diffusion of dissolved components from particle to the glass matrix and depends on the glass viscosity as a function of temperature [34]. This area can be imagined as boundary crust or buffer area between the glass matrix and the particle. The  $Eu^{2+}$  PL spectrum measured in the  $BaO$ - $CaO$ - $2SiO_2$ : $Eu(1 \text{ at.}\%)$  glass systems [35] was spread over approximately 400–600 nm region centered at about 450–500 nm (depended on the glass composition).

The origin of the G5 peak at 470 nm is rather obscure. It is totally absent (or hidden with lowered intensity) in the sample 5. The G5 could be produced by the  $Eu^{2+}$  ions inside the glass medium nearest to the particle (boundary crust or buffer area) or by some defect, for example, oxygen centers, originating from the samples hydrolysis either with their own crystallization water or the water released during the synthesis in accordance with Eq. (1) [18,36,37]. Remarkably, according to the single Gaussians areas listed in Table III, the G3 band is dominating in the sample 5 and nearly dominating in the sample 4, where the G5 is of the same strength. It is clearly seen in Fig. 7 as well. This can be the sign of relatively strong dissolution of the  $BaI_2$ : $Eu$  in the glass matrix unless the  $Eu^{2+}$  emission is concentration quenched in the ceramics particles.

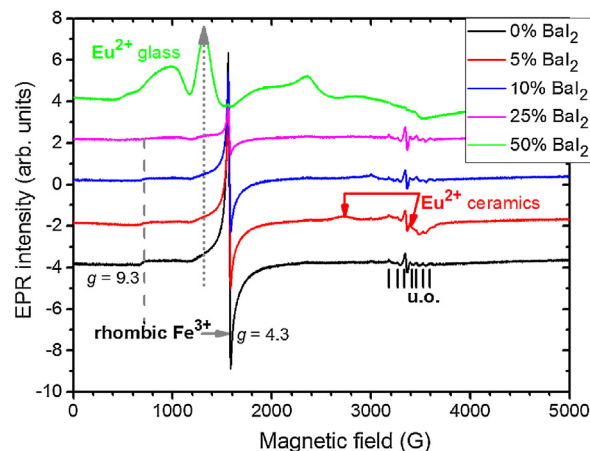


**Fig. 8** – EPR spectra measured in glass ceramics samples 1–5 at  $T = 100$  K.  $Eu^{2+}$  signals in glass (one of the transitions is indicated by short dotted arrow) and ceramic part are indicated. Rhombic  $Fe^{3+}$  signals are also indicated. “u.o.” means unknown origin of some unexpected impurity.

To study the  $Eu^{2+}$  ions incorporation into the  $BaI_2$  lattice and the glass matrix in the glass ceramics EPR method was used. EPR spectra of the glass ceramics samples 1–5 are shown in Fig. 8.

All the spectra contain some signals obviously coming from unexpected impurity of unknown origin (“u.o.”). Besides, they demonstrate the presence of the signals characteristic for rhombic  $Fe^{3+}$  observed at the specific  $g$  factors,  $g_1 = 4.3$  and  $g_2 = 9.3$  (for more details see e.g., [38]). The presence of the rhombic  $Fe^{3+}$  can be explained by the use of porcelain crucibles ( $Fe_2O_3$  can be found in such materials [39]) for the glass synthesis.

Note, that the glass ceramics with low content (<25%) of the barium iodide demonstrates no visible  $Eu^{2+}$  signals except the sample 1 as it is shown in Fig. 9. It exhibits some weak resonances which might be attributed to the  $Eu^{2+}$ -like signals if compared with the  $BaI_2$ : $Eu$  (20%) powder [18] within the

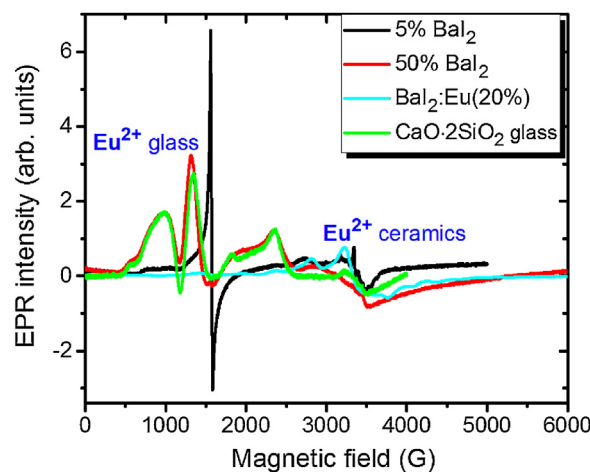


**Fig. 9** – EPR spectra measured in glass ceramics samples 1 and 5,  $BaI_2$ : $Eu(20\%)$  powder [18] and  $CaO$ : $2SiO_2$ : $Eu(1 \text{ at.}\%)$  glass [35] at  $T = 100$  K.

**Table 3 – Gaussian parameters obtained from fit in Fig.**

Sample	Gi	E <sub>i</sub> , eV	FWHM <sub>i</sub> , eV	A <sub>i</sub> , a. u.
Sample 4	G1	2.37 ± 0.05 (523 nm)	0.17 ± 0.05	0.03 ± 0.01
	G2	2.52 ± 0.05 (492 nm)	0.12 ± 0.05	0.07 ± 0.01
	G3	2.74 ± 0.05 (453 nm)	0.18 ± 0.05	0.11 ± 0.01
	G4	2.94 ± 0.05 (422 nm)	0.21 ± 0.05	0.05 ± 0.01
	G5	2.64 ± 0.05 (470 nm)	0.13 ± 0.05	0.11 ± 0.01
Sample 5	G1	2.37 ± 0.05 (523 nm)	0.2 ± 0.05	0.06 ± 0.01
	G2	2.52 ± 0.05 (492 nm)	0.16 ± 0.05	0.08 ± 0.01
	G3	2.74 ± 0.05 (453 nm)	0.23 ± 0.05	0.24 ± 0.01
	G4	2.94 ± 0.05 (422 nm)	0.21 ± 0.05	0.08 ± 0.01

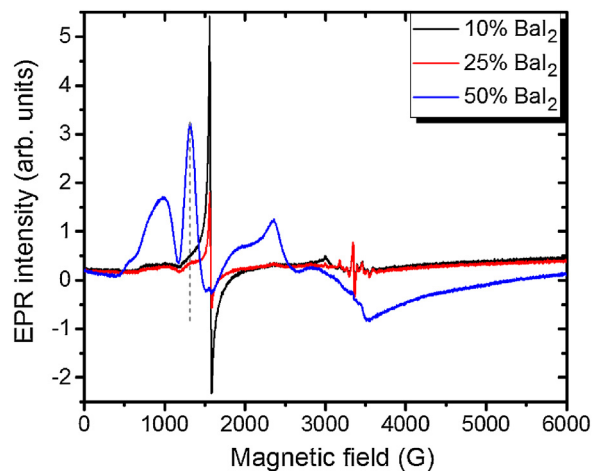


**Fig. 10 – EPR spectra measured in glass ceramics samples 3, 4 and 5 at  $T = 100$  K. A vertical dashed line stresses the 1250 G  $\text{Eu}^{2+}$  glass spectrum transition.**

2500–4000 magnetic field range. However, it is hard to proof on the basis of the presented data. The observed signals could originate not from the glass ceramics but from the  $\text{BaI}_2$  powder remnants “stuck” to the glass ceramics sample.

The sample 5 exhibits  $\text{Eu}^{2+}$  spectrum typical for glass (see Fig. 9). The spectrum measured in  $\text{CaO}\cdot 2\text{SiO}_2\cdot \text{Eu}(1\text{ at.}\%)$  glass [35] is shown in contrast as well. It is not excluded that, some signals may come from the  $\text{BaI}_2$  particles, however, strongly overlapped with the dominating glass ones. This may also confirm, at least, partial dissolution of the  $\text{BaI}_2$  particles in the glass matrix or partial decomposition on the  $\text{BaI}_2$  and  $\text{EuI}_2$ , discussed in detail above. The  $\text{Eu}^{2+}$  EPR signal from the  $\text{EuI}_2$  is expected to be very broad because of strong dipolar and exchange interactions [38], lost in the background. Fig. 10 demonstrates clearly the presence of the glass  $\text{Eu}^{2+}$  spectrum also in the sample 4 if one could judge from the transition at about 1250 G emphasized with a dashed vertical line. But it should have approximately 20 times lower intensity.

To examine other possible europium ions charge state and incorporation in the “really” europium containing sample 5 it has been exposed to 442 nm laser irradiation. The corresponding spectra are shown in Fig. 11.

Remarkably, the irradiation with the 442 nm laser forces the  $\text{Eu}^{2+}$  glass spectrum to lose its initial intensity. The spectrum measured 10 min after the irradiation shows the same signal as the one measured immediately after the irradiation.

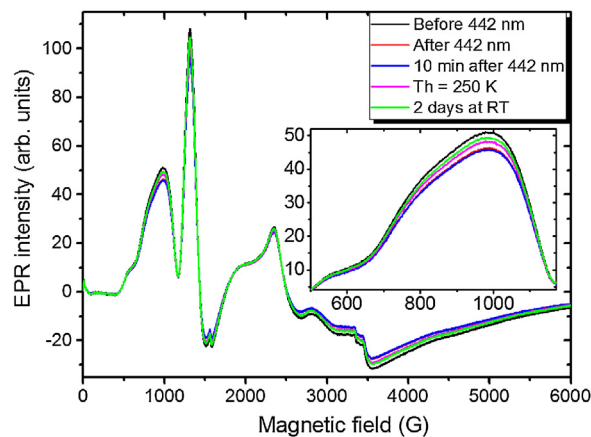


**Fig. 11 – EPR spectra measured in the sample 5 before 442 nm laser irradiation, immediately after, 10 min after the irradiation, after annealing at the heating temperature  $T_h = 250$  K, and after two days at room temperature (RT). All spectra have been measured at  $T = 25$  K in turn.**

Annealing at 250 K for 5 min then results in partial recover of the intensity but not to the full measure. Even after two days at RT the same spectrum as the one obtained after the annealing at 250 K was measured. The only way to observe such changes is the partial  $\text{Eu}^{2+} \rightarrow \text{Eu}^{3+}$  charge transfer in the glass matrix.

No signals which might be attributed to paramagnetic oxygen centers, like  $\text{O}^-$  defects (see e.g. [40,41]) were observed in EPR spectra (see Fig. 8). Predominating  $\text{Eu}^{2+}$  glass spectra make evidence of the  $\text{BaI}_2\text{:Eu}$  strong decomposition in the glass matrix.

## Conclusions

The paper reports a common approach to the  $\text{Eu}^{2+}$ -doped glass ceramics synthesis from the  $\text{BaI}_2\text{:Eu}$  powder. Different levels of the  $\text{BaI}_2$  content were tried but, unfortunately, only the samples nominally supplied by the 25 and 50 wt.% appeared to demonstrate its presence as well as hydrated barium iodide by direct observation of the corresponding XRD reflections. The presence of  $\text{BaI}_2$  particles inside the glass matrix was also confirmed by SEM. Increased rigidity of the particles in the glass ceramics has been proven by microstress measurements ( $\epsilon$  becomes approximately 3 times lower in the glass ceramics than in the barium iodide powder itself).



Photoluminescence spectra are single band in the Ba<sub>2</sub>:Eu powder. However, they are getting very complex, composed of at least 5 bands in the 25 wt.% Ba<sub>2</sub> and 4 bands in the 50 wt.% Ba<sub>2</sub> samples: 422 nm, 453 nm, 492 nm, 523 nm common for both samples and the 470 nm one, observed only in the 25 wt.% Ba<sub>2</sub>. The 422 nm band was referred to the Eu<sup>2+</sup> in the Ba<sub>2</sub> particles. Other bands were referred either to the Eu<sup>2+</sup> in EuI<sub>2</sub> (byproduct of the glass ceramics synthesis) or glass matrix (glass-ceramics boundary), or some non-paramagnetic oxygen-related centers. The 453 nm band is dominating in both samples indicating strong possibility of the Ba<sub>2</sub> dissolution in the glass. No PL signals were measured in other glass ceramics with the Ba<sub>2</sub> content lower than 25 wt.%.

EPR measurements report the presence of the Eu<sup>2+</sup> ions in the samples with the 25 and 50 wt.% of Ba<sub>2</sub>. They are very strong and clearly resolved only in the latter exhibiting features characteristic for glass. This also benefits to the supposition of the Ba<sub>2</sub> decomposition and Eu<sup>2+</sup> ions incorporation into the glass matrix or ceramics-glass boundaries especially in the 25 wt.% Ba<sub>2</sub> sample where the ceramics particles are ball-shaped. Nevertheless, some small amount of the Eu<sup>2+</sup> is expected to be located in the Ba<sub>2</sub> ceramic particles in the glass. Their signal is getting lost in the background of the strong transitions of the Eu<sup>2+</sup> ions in the glass. The 442 nm laser light irradiation resulted in decrease of the Eu<sup>2+</sup> intensity obviously engaging the permanent Eu<sup>2+</sup> → Eu<sup>3+</sup> charge state transformation. The glass ceramics samples contained also rhombic Fe<sup>3+</sup> which EPR intensity is dependent on the Ba<sub>2</sub>:Eu content. It was explained by the inclusion of the Ba<sub>2</sub> particles and partial decomposition of the barium iodide in the glass matrix along with the Fe<sup>3+</sup> → Fe<sup>2+</sup> charge state transformation caused by the Eu<sup>2+</sup> → Eu<sup>3+</sup> oxidation or the decomposition of the I<sub>3</sub><sup>-</sup> to I<sub>2</sub> or similar.

In general, the possible mechanism of the Ba<sub>2</sub>:Eu glass ceramics fabrication was proposed and analyzed in detail. It is expected to be applicable to the synthesis of glass ceramic materials based on the wide range of other halide compounds after appropriate modification. The proposed approach can be subsequently expanded to obtain other promising materials, such as SrI<sub>2</sub>, CaI<sub>2</sub>, MgI<sub>2</sub>, LaBr<sub>3</sub> in the glass ceramics form, but this requires understanding of the processes that occur during the glass ceramics preparation. Even despite the long duration of glass ceramics synthesis, technologically it is still simpler and less expensive than growing a single crystal or producing optically transparent ceramics.

## Acknowledgements

Authors gratefully acknowledge the financial support of the Belarusian State Program of Scientific Research "Photonics, opto- and microelectronics" (No 1.2.03), the Ministry of Education, Youth and Sports of Czech Republic under projects LO1409 and CZ.02.1.01/0.0/0.0/16\_013/0001406 and mobility project "Development and enhancement of luminescent materials for multipurpose applications" of Czech Academy of Sciences and National Academy of Sciences of Belarus (No NASB-20-03).

## REFERENCES

- [1] D. De Faoite, L. Hanlon, O. Roberts, A. Ulyanov, S. McBreen, I. Tobin, K.T. Stanton, Development of glass-ceramic scintillators for gamma-ray astronomy, *J. Phys. Conf. Ser.* (2015) 0120021–0120026.
- [2] M. Nikl, A. Yoshikawa, Recent R&D trends in inorganic single-crystal scintillator materials for radiation detection, *Adv. Opt. Mater.* 3 (2015) 463–481, <http://dx.doi.org/10.1002/adom.201400571>.
- [3] G. Blasse, Scintillator materials, *Chem. Mater.* 6 (1994) 1465–1475, <http://dx.doi.org/10.1021/cm00045a002>.
- [4] H. Lin, T. Hu, Y. Cheng, M. Chen, Y. Wang, Glass ceramic phosphors: towards long-lifetime high-power white light-emitting-diode applications – a review, *Laser Photon. Rev.* 12 (2018) 1700344, <http://dx.doi.org/10.1002/lpor.201700344>.
- [5] M. Tyagi, M. Zhuravleva, C.L. Melcher, Theoretical and experimental characterization of promising new scintillators: Eu<sup>2+</sup> doped CsCaCl<sub>3</sub> and CsCaI<sub>3</sub>, *J. Appl. Phys.* 113 (2013) 203504, <http://dx.doi.org/10.1063/1.4807401>.
- [6] C. Struebing, J.Y. Chong, G. Lee, M. Zavala, A. Erickson, Y. Ding, C.L. Wang, Y. Diawara, R. Engels, B. Wagner, Z. Kang, A neutron scintillator based on transparent nanocrystalline CaF<sub>2</sub>:Eu glass ceramic, *Appl. Phys. Lett.* 108 (2016) 153106, <http://dx.doi.org/10.1063/1.4945999>.
- [7] C. Greskovich, S. Duclos, Ceramic scintillators, *Annu. Rev. Mater. Sci.* 27 (1997) 69–88, <http://dx.doi.org/10.1146/annurev.matsci.27.1.69>.
- [8] Y. Tratsiak, M. Korzhik, A. Fedorov, G. Dosovitsky, O. Akimova, S. Belus, M. Fasoli, A. Vedda, V. Mechinsky, E. Trusova, On the stabilization of Ce, Tb, and Eu ions with different oxidation states in silica-based glasses, *J. Alloys Compd.* 797 (2019) 302–308, <http://dx.doi.org/10.1016/j.jallcom.2019.05.105>.
- [9] E. Trusova, A. Vaitkevicius, Y. Tratsiak, M. Korjik, P. Mengucci, D. Rinaldi, L. Montalto, V. Marciulionyte, G. Tamulaitis, Barium and lithium silicate glass ceramics doped with rare earth ions for white LEDs, *Opt. Mater. (Amst.)* 84 (2018) 459–465, <http://dx.doi.org/10.1016/j.optmat.2018.07.030>.
- [10] Y. Tratsiak, M. Korjik, A. Fedorov, G. Dosovitsky, O. Akimova, E. Gordienko, M. Fasoli, V. Mechinsky, A. Vedda, F. Moretti, E. Trusova, Luminescent properties of binary MO<sub>2</sub>SiO<sub>2</sub> (M = Ca<sup>2+</sup>, Sr<sup>2+</sup>, Ba<sup>2+</sup>) glasses doped with Ce<sup>3+</sup>, Tb<sup>3+</sup> and Dy<sup>3+</sup>, *J. Alloys Compd.* 765 (2018) 207–212, <http://dx.doi.org/10.1016/j.jallcom.2018.06.210>.
- [11] J. Ma, C.Z. Chen, D.G. Wang, J.H. Hu, Synthesis, characterization and in vitro bioactivity of magnesium-doped sol-gel glass and glass-ceramics, *Ceram. Int.* 37 (2011) 1637–1644, <http://dx.doi.org/10.1016/j.ceramint.2011.01.043>.
- [12] G. Gorni, R. Balda, J. Fernández, I. Iparraguirre, J.J. Velázquez, Y. Castro, L. Pascual, G. Chen, M. Sundararajan, M.J. Pascual, A. Durán, Oxyfluoride glass-ceramic fibers doped with Nd<sup>3+</sup>: structural and optical characterization, *CrystEngComm* 19 (2017) 6620–6629, <http://dx.doi.org/10.1039/c7ce01380a>.
- [13] G. Gorni, M.J. Pascual, A. Caballero, J.J. Velázquez, J. Mosa, Y. Castro, A. Durán, Crystallization mechanism in sol-gel oxyfluoride glass-ceramics, *J. Non. Cryst. Solids* 501 (2018) 145–152, <http://dx.doi.org/10.1016/j.jnoncrsol.2018.01.031>.
- [14] J. Huang, X. Hu, J. Shen, D. Wu, C. Yin, R. Xiang, C. Yang, X. Liang, W. Xiang, Facile synthesis of a thermally stable Ce<sup>3+</sup>:Y<sub>3</sub>Al<sub>5</sub>O<sub>12</sub> phosphor-in-glass for white LEDs, *CrystEngComm* 17 (2015) 7079–7085, <http://dx.doi.org/10.1039/c5ce01365h>.
- [15] J. Deubener, M. Allix, M.J. Davis, A. Duran, T. Höche, T. Honma, T. Komatsu, S. Krüger, I. Mitra, R. Müller, S. Nakane, M.J. Pascual, J.W.P. Schmelzer, E.D. Zannotto, S. Zhou, Updated

- definition of glass-ceramics, *J. Non. Cryst. Solids* 501 (2018) 3–10, <http://dx.doi.org/10.1016/j.jnoncrysol.2018.01.033>.
- [16] S. Fujita, S. Tanabe, Fabrication, microstructure and optical properties of  $\text{Er}^{3+}$ :YAG glass-ceramics, *Opt. Mater. (Amst.)* 32 (2010) 886–890, <http://dx.doi.org/10.1016/j.optmat.2010.01.014>.
- [17] Z. Yan, G. Gundiah, G.A. Bizarri, E.C. Samulon, S.E. Derenzo, E.D. Bourret-Courchesne,  $\text{Eu}^{2+}$ -activated  $\text{BaCl}_2$ ,  $\text{BaBr}_2$  and  $\text{BaI}_2$  scintillators revisited, *Nucl. Instrum. Methods Phys. Res. Sect. A Accel. Spectrom. Detect. Assoc. Equip.* 735 (2014) 83–87.
- [18] T. Salamakha, M. Buryi, Y. Tratsiak, Effect of Eu-doping on optical, structural and morphological properties of  $\text{BaI}_2 \cdot n\text{H}_2\text{O}$  powders, *Opt. Mater. (Amst.)* 78 (2018) 352–359, <http://dx.doi.org/10.1016/j.optmat.2018.02.044>.
- [19] A. Schleife, X. Zhang, Q. Li, P. Erhart, D. Åberg, Excitons in scintillator materials: Optical properties and electron-energy loss spectra of  $\text{NaI}$ ,  $\text{LaBr}_3$ ,  $\text{BaI}_2$ , and  $\text{SrI}_2$ , *J. Mater. Res.* 32 (2017) 56–63.
- [20] E.V. Van Loef, C.M. Wilson, N.J. Cherepy, G. Hull, S.A. Payne, W.S. Choong, W.W. Moses, K.S. Shah, Crystal growth and scintillation properties of strontium iodide scintillators, *IEEE Trans. Nucl. Sci.* 56 (2009) 869–872.
- [21] T. Salamakha, Y. Tratsiak, E. Trusova, New glass ceramic luminescent materials for a wide application, in: *Şişecam Int. Glas. Conf. Comb. with 34 Şişecam Glas. Symp., Istanbul, 2019*, p. 187.
- [22] E.V. Tretyak, G.P. Shevchenko, T.A. Solomakha, M.V. Korzhik, Effect of precursor morphology on the structural properties, optical absorption, and luminescence of  $\text{BaI}_2:\text{Eu}^{2+}, \text{Eu}^{3+}$ , *Inorg. Mater.* 53 (2017) 307–312.
- [23] G.K. Williamson, W.H. Hall, X-ray line broadening from filed aluminium and wolfram, *Acta Metall.* 1 (1953) 22–31, [http://dx.doi.org/10.1016/0001-6160\(53\)90006-6](http://dx.doi.org/10.1016/0001-6160(53)90006-6).
- [24] M. Zhuravleva, L. Stand, H. Wei, C. Hobbs, L.A. Boatner, J.O. Ramey, K. Shah, A. Burger, E. Rowe, P. Bhattacharya, E. Tupitsyn, C.L. Melcher, Hygroscopicity evaluation of halide scintillators, *IEEE Nucl. Sci. Symp. Conf. Rec.* (2013) 1–5, <http://dx.doi.org/10.1109/NSSMIC.2013.6829669>.
- [25] K. Nakamoto, *Infrared and Raman Spectra of Inorganic and Coordination Compounds*, John Wiley & Sons, Ltd., 2006, <http://dx.doi.org/10.1002/9780470027325.s4104>.
- [26] L. Wang, X. Wang, M. Xu, D. Chen, J. Sun, Layer-by-layer assembled microgel films with high loading capacity: Reversible loading and release of dyes and nanoparticles, *Langmuir* 24 (2008) 1902–1909, <http://dx.doi.org/10.1021/la7031048>.
- [27] K. Biswas, A.D. Sontakke, R. Sen, K. Annappurna, Luminescence properties of dual valence Eu doped nano-crystalline  $\text{BaF}_2$  embedded glass-ceramics and observation of  $\text{Eu}^{2+} \rightarrow \text{Eu}^{3+}$  energy transfer, *J. Fluoresc.* 22 (2012) 745–752.
- [28] Q. Luo, X. Qiao, X. Fan, S. Liu, H. Yang, X. Zhang, Reduction and luminescence of europium ions in glass ceramics containing  $\text{SrF}_2$  nanocrystals, *J. Non. Cryst. Solids* 354 (2008) 4691–4694.
- [29] M.I. Danilkin, A.P. Belousov, S.O. Klimonskii, V.D. Kuznetsov, A.L. Lust, V.N. Nikiforov, L.N. Paama, I.K. Pammo, V.O. Seeman, Formation of  $\text{Eu}^{2+}$  and  $\text{Eu}^{3+}$  centers in synthesis of  $\text{CaF}_2:\text{Eu}$  luminophores, *J. Appl. Spectrosc.* 74 (2007) 858–865, <http://dx.doi.org/10.1007/s10812-007-0133-5>.
- [30] L. Havlák, J. Bárta, M. Buryi, V. Jarý, E. Mihóková, V. Laguta, P. Boháček, M. Nikl,  $\text{Eu}^{2+}$  Stabilization in YAG structure: optical and electron paramagnetic resonance study, *J. Phys. Chem. C* 120 (2016) 21751–21761, <http://dx.doi.org/10.1021/acs.jpcc.6b06397>.
- [31] P. Lecoq, A. Gektin, M. Korzhik, Scintillation and inorganic scintillators, *Inorg. Scintill. Detect. Syst. Phys. Princ. Cryst. Eng.* (2017) 1–41.
- [32] L. Wang, S. Wang, X. Zhao, J. Sun, Stability, structure and fluorescence spectra of high-pressure-treated  $\text{Eu}^{2+}$  iodides, *J. Alloys Compd.* 225 (1995) 174–177.
- [33] E. Rogers, P. Dorenbos, J.T.M. De Haas, E. Van Der Kolk, Experimental study of the  $4f^n \rightarrow 4f^n$  and  $4f^n \rightarrow 4f^{n-1}5d^1$  transitions of the lanthanide diiodides  $\text{LnI}_2$  ( $\text{Ln} = \text{Nd}, \text{Sm}, \text{Eu}, \text{Dy}, \text{Tm}, \text{Yb}$ ), *J. Phys. Condens. Matter.* 24 (2012) 275502, <http://dx.doi.org/10.1088/0953-8984/24/27/275502>.
- [34] Y. Tratsiak, E. Trusova, Y. Bokshits, M. Korjik, A. Vaitkevicius, G. Tamulaitis, Garnet-type crystallites, their isomorphism and luminescence properties in glass ceramics, *CrystEngComm* 21 (2019) 687–693, <http://dx.doi.org/10.1039/C8CE01547C>.
- [35] Y. Tratsiak, M. Buryi, V. Babin, M. Korjik, E. Trusova, The effect of binary glass composition on the Eu-ions luminescence properties, *Opt. Mater. (Amst.)* 94 (2019) 356–362, <http://dx.doi.org/10.1016/j.optmat.2019.06.011>.
- [36] V. Pankratov, A.I. Popov, L. Shirmane, A. Kotlov, G.A. Bizarri, A. Burger, P. Bhattacharya, E. Tupitsyn, E. Rowe, V.M. Buliga, R.T. Williams, Luminescence and ultraviolet excitation spectroscopy of  $\text{SrI}_2$  and  $\text{SrI}_2:\text{Eu}^{2+}$ , *Radiat. Meas.* 56 (2013) 13–17.
- [37] V.V. Vistovskyy, A.V. Zhyshkovych, Y.M. Chornodolskyy, O.S. Myagkota, A. Gloskovskii, A.V. Gektin, A.N. Vasil'Ev, P.A. Rodnyi, A.S. Voloshinovskii, Self-trapped exciton and core-valence luminescence in  $\text{BaF}_2$  nanoparticles, *J. Appl. Phys.* 114 (2013) 1943061–1943067.
- [38] J.R. Pilbrow, *Transition Ion Electron Paramagnetic Resonance*, Clarendon Press, 1990, <http://dx.doi.org/10.1002/bbpc.19910951036>.
- [39] N.T. Muriithi, K.B. Karoki, A.N. Gachanja, Chemical and mineral analyses of Mwea clays, *Int. J. Phys. Sci.* 7 (2012) 5865–5869, <http://dx.doi.org/10.5897/IJPS11.1103>.
- [40] M. Buryi, D.A. Spassky, J. Hybler, V. Laguta, M. Nikl, Electron Spin Resonance study of charge trapping in  $\alpha$ - $\text{ZnMoO}_4$  single crystal scintillator, *Opt. Mater. (Amst.)* 47 (2015) 244–250, <http://dx.doi.org/10.1016/j.optmat.2015.05.032>.
- [41] M. Buryi, P. Boháček, K. Chernenko, A. Krasnikov, V.V. Laguta, E. Mihokova, M. Nikl, S. Zazubovich, Luminescence and photo-thermally stimulated defect-creation processes in  $\text{Bi}^{3+}$ -doped single crystals of lead tungstate, *Phys. Status Solidi Basic Res.* 253 (2016) 895–910, <http://dx.doi.org/10.1002/pssb.201552697>.